Axial nucleon form factors from lattice QCD

C. Alexandrou,[1,2] M. Brinet,[3] J. Carbonell,[3] M. Constantinou,[1] P. A. Harraud,[3]
P. Guichon,[4] K. Jansen,[5] T. Korzec,[1,6] and M. Papinutto[3]

[1]*Department of Physics, University of Cyprus, P.O. Box 20537, 1678 Nicosia, Cyprus*
[2]*Computation-based Science and Technology Research Center, Cyprus Institute, 20 Kavafi Str., Nicosia 2121, Cyprus*
[3]*Laboratoire de Physique Subatomique et Cosmologie, UJF/CNRS/IN₂P₃, 53 avenue des Martyrs, 38026 Grenoble, France*
[4]*CEA-Saclay, IRFU/Service de Physique Nucléaire, 91191 Gif-sur-Yvette, France*
[5]*NIC, DESY, Platanenallee 6, D-15738 Zeuthen, Germany*
[6]*Institut für Physik Humboldt Universität zu Berlin, Newtonstrasse 15, 12489 Berlin, Germany*
(Received 3 December 2010; published 14 February 2011)

We present results on the nucleon axial form factors within lattice QCD using two flavors of degenerate twisted mass fermions. Volume effects are examined using simulations at two volumes of spatial length $L = 2.1$ fm and $L = 2.8$ fm. Cut-off effects are investigated using three different values of the lattice spacings, namely $a = 0.089$ fm, $a = 0.070$ fm and $a = 0.056$ fm. The nucleon axial charge is obtained in the continuum limit and chirally extrapolated to the physical pion mass enabling comparison with experiment.

I. INTRODUCTION

The nucleon (N) form factors are fundamental hadronic observables that probe the structure of the nucleon. Experiments to measure the electromagnetic nucleon form factors have been carried out since the 1950s. A new generation of experiments using polarized beams and targets is currently under way at major facilities in order to measure the nucleon form factors more accurately and at higher values of the momentum transfer. The nucleon form factors connected to the axial vector current are more difficult to measure and therefore less accurately known than its electromagnetic form factors. As in the electromagnetic case the nucleon matrix element of the axial vector current is written in terms of two Lorenz invariant form factors, the axial form factor $G_A(q^2)$ and the induced pseudoscalar form factor, $G_p(q^2)$ where q^2 is the momentum transfer squared. The nucleon axial charge $g_A = G_A(0)$, which can be determined from β-decay, is known to a high precision. The q^2-dependence of $G_A(q^2)$ has been studied from neutrino scattering [1] and pion electroproduction [2,3] processes. The nucleon induced pseudoscalar form factor, $G_p(q^2)$, is even less well known. Muon capture at low q^2 values [4] and pion electroproduction for larger Q^2 [2,3] are the main experimental sources of information for $G_p(Q^2)$. Both $G_A(q^2)$ and $G_p(q^2)$ have been discussed within chiral effective theories [5,6]. In this work we present results on these form factors obtained in lattice QCD using two degenerate light quarks ($N_F = 2$) in the twisted mass formulation [7].

Twisted mass fermions [8] provide an attractive formulation of lattice QCD that allows for automatic $\mathcal{O}(a)$ improvement, infrared regularization of small eigenvalues and fast dynamical simulations. For the calculation of the nucleon form factors in which we are interested in this work, the automatic $\mathcal{O}(a)$ improvement is particularly relevant since it is achieved by tuning only one parameter in the action, requiring no further improvements on the operator level.

The action for two degenerate flavors of quarks in twisted mass QCD is given by

$$S = S_g + a^4 \sum_x \bar{\chi}(x)[D_W + m_{\text{crit}} + i\gamma_5\tau^3\mu]\chi(x), \quad (1)$$

where D_W is the Wilson Dirac operator and we use the tree-level Symanzik improved gauge action S_g [9]. The quark fields χ are in the so-called "twisted basis" obtained from the "physical basis" at maximal twist by a simple transformation:

$$\psi = \frac{1}{\sqrt{2}}[\mathbb{1} + i\tau^3\gamma_5]\chi \text{ and } \bar{\psi} = \bar{\chi}\frac{1}{\sqrt{2}}[\mathbb{1} + i\tau^3\gamma_5]. \quad (2)$$

We note that, in the continuum, this action is equivalent to the standard QCD action. A crucial advantage is the fact that by tuning a single parameter, namely, the bare untwisted quark mass to its critical value m_{cr}, a wide class of physical observables are automatically $\mathcal{O}(a)$ improved [7]. A disadvantage is the explicit flavor symmetry breaking. In a recent paper we have checked that this breaking is small for the baryon observables under consideration in this work and for the lattice spacings that we use [10–14]. To extract the nucleon FFs we need to evaluate the nucleon matrix elements $\langle N(p', s')|A^a_\mu|N(p, s)\rangle$, where $|N(p', s')\rangle$, $|N(p, s)\rangle$ are nucleon states with final (initial) momentum $p'(p)$ and spin $s'(s)$. Because of its isovector nature, the axial vector current, defined by

$$A^a_\mu(x) = \bar{\psi}(x)\gamma_\mu\gamma_5\frac{\tau^a}{2}\psi(x), \quad (3)$$

receives contributions only from the connected diagram for $a = 1$, 2 and up to $\mathcal{O}(a^2)$ for $a = 3$ [15]. Simulations

including a dynamical strange quark are also available within the twisted mass formulation. Comparison of the nucleon mass obtained with two dynamical flavors and the nucleon mass including a dynamical strange quark has shown negligible dependence on the dynamical strange quark [16]. We therefore expect the results on the nucleon form factors to show little sensitivity on a dynamical strange quark as well.

The axial current matrix element of the nucleon $\langle N(p', s')|A_\mu^a(0)|N(p, s)\rangle$ can be expressed in terms of the form factors G_A and G_p as

$$\langle N(p', s')|A_\mu^3|N(p, s)\rangle = i\left(\frac{m_N^2}{E_N(\mathbf{p}')E_N(\mathbf{p})}\right)^{1/2} \bar{u}_N(p', s')$$

$$\times \left[G_A(q^2)\gamma_\mu\gamma_5 + \frac{q_\mu\gamma_5}{2m_N}G_p(q^2)\right]\frac{1}{2}u_N(p, s). \quad (4)$$

where $u_N(p, s)$ denotes the nucleon spinor.

In this work we consider simulations at three values of the coupling constant spanning lattice spacings from about 0.05 fm to 0.09 fm. This enables us to obtain results in the continuum limit. We find that cutoff effects are small for this range of lattice spacings. We also examine finite size effects on the axial form factors by comparing results on two lattices of spatial length $L = 2.1$ fm and $L = 2.8$ fm [17–19].

II. LATTICE EVALUATION

A. Correlation functions

The proton interpolating field in the physical basis is given by

$$J(x) = \epsilon^{abc}[u^{a\top}(x)\mathcal{C}\gamma_5 d^b(x)]u^c(x) \quad (5)$$

and can be written in the twisted basis at maximal twist as

$$\tilde{J}(x) = \frac{1}{\sqrt{2}}[\mathbb{1} + i\gamma_5]\epsilon^{abc}[\tilde{u}^{a\top}(x)\mathcal{C}\gamma_5\tilde{d}^b(x)]\tilde{u}^c(x). \quad (6)$$

The transformation of the axial vector current, $A_\mu^a(x)$, to the twisted basis leaves the form of $A_\mu^3(x)$ unchanged. The axial renormalization constant Z_A is determined nonperturbatively in the RI'-MOM scheme using two approaches [20–23] both of which yield consistent values. We use the values of Z_A found in the latter approach [22], which employs a momentum source [24] and a perturbative subtraction of $\mathcal{O}(a^2)$ terms [25,26]. This subtracts the leading cutoff effects yielding only a very weak dependence of Z_A on $(ap)^2$ for which the $(ap)^2 \to 0$ limit can be reliably taken. It was also shown with high accuracy that the quark mass dependence of Z_A is negligible. We find the values

$$Z_A = 0.757(3), 0.776(3), 0.789(3) \quad (7)$$

at $\beta = 3.9, 4.05$ and 4.2, respectively. For comparison, the values obtained in Ref. [21] are

$$Z_A = 0.746(6), 0.772(6) \quad (8)$$

for $\beta = 3.9$ and $\beta = 4.05$, respectively. In this work we use the values for Z_A given in Eq. (7).

In order to increase the overlap with the proton state and decrease overlap with excited states we use Gaussian smeared quark fields [27,28] for the construction of the interpolating fields:

$$q_{\text{smear}}^a(t, \vec{x}) = \sum_{\vec{y}} F^{ab}(\vec{x}, \vec{y}; U(t))q^b(t, \vec{y}),$$

$$F = (\mathbb{1} + \alpha H)^n,$$

$$H(\vec{x}, \vec{y}; U(t)) = \sum_{i=1}^3 [U_i(x)\delta_{x, y-\hat{\imath}} + U_i^\dagger(x - \hat{\imath})\delta_{x, y+\hat{\imath}}]. \quad (9)$$

In addition, we apply APE-smearing to the gauge fields U_μ entering the hopping matrix H. The smearing parameters are the same as those used for our calculation of baryon masses with α and n optimized for the nucleon ground state [13]. The values are $\alpha = 4.0$ and $n = 50, 70$ and 90 for $\beta = 3.9, 4.05$ and 4.2, respectively.

In order to calculate the nucleon matrix element of Eq. (4) we calculate the two-point and three-point functions defined by

$$G(\vec{q}, t_f) = \sum_{\vec{x}_f} e^{-i\vec{x}_f \cdot \vec{q}}\Gamma_{\beta\alpha}^0\langle J_\alpha(t_f, \vec{x}_f)\bar{J}_\beta(t_i, \vec{x}_i)\rangle$$

$$G^\mu(\Gamma^\nu, \vec{q}, t) = \sum_{\vec{x}, \vec{x}_f} e^{i\vec{x} \cdot \vec{q}}\Gamma_{\beta\alpha}^\nu\langle J_\alpha(t_f, \vec{x}_f)A^\mu(t, \vec{x})\bar{J}_\beta(t_i, \vec{x}_i)\rangle, \quad (10)$$

where Γ^0 and Γ^k are the projection matrices:

$$\Gamma^0 = \frac{1}{4}(\mathbb{1} + \gamma_0), \qquad \Gamma^k = i\Gamma^0\gamma_5\gamma_k. \quad (11)$$

The kinematical setup that we used is illustrated in Fig. 1: We create the nucleon at $t_i = 0$, at $\vec{x}_i = 0$ (source) and annihilate it at a later time t_f with $\vec{p}' = 0$ (sink). The current couples to a quark at an intermediate time t. For our kinematics $\vec{q} = -\vec{p}$. From now on all quantities are given in Euclidean space and where $Q^2 = -q^2$ is the Euclidean momentum transfer squared. The leading time dependence of the Euclidean time evolution and the overlap factors cancel in the ratio

$$R^\mu(\Gamma, \vec{q}, t) = \frac{G^\mu(\Gamma, \vec{q}, t)}{G(\vec{0}, t_f)}\sqrt{\frac{G(\vec{p}_i, t_f - t)G(\vec{0}, t)G(\vec{0}, t_f)}{G(\vec{0}, t_f - t)G(\vec{p}_i, t)G(\vec{p}_i, t_f)}},$$

$$(12)$$

yielding a time-independent quantity

$$\lim_{t_f - t \to \infty} \lim_{t - t_i \to \infty} R^\mu(\Gamma, \vec{q}, t) = \Pi^\mu(\Gamma, \vec{q}). \quad (13)$$

We refer to the range of t-values where this asymptotic behavior is observed within our statistical precision as the plateau range. As mentioned already, only the connected diagram contributes. It is calculated by performing sequential inversions through the sink yielding the form factors at
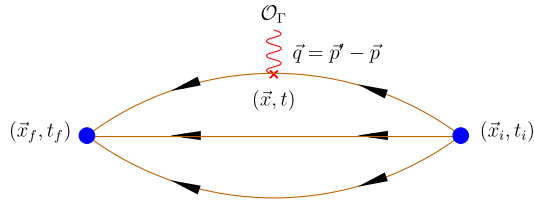
FIG. 1 (color online). Connected nucleon three-point function.

all possible momentum transfers and current orientation μ. Since we use sequential inversions through the sink we need to fix the sink-source separation. Statistical errors increase rapidly as we increase the sink-source separation. Therefore we need to choose the smallest possible separation still ensuring that the nucleon ground state dominates when measurements are made at different values of t. In order to check that a sink-source time separation of ~ 1 fm is sufficient for the isolation of the nucleon ground state we compare the results at $\beta = 3.9$ obtained with $t_f/a = 12$ i.e. $t_f \sim 1$ fm with those obtained when we increase the value of $t_f/a = 14$ [19]. As can be seen in Fig. 2, where we plot $R^\mu(\Gamma, \vec{q}, t)$, data are compatible yielding the same plateau value for the two time separations. This means that the shorter sink-source separation is sufficient and the ground state of the nucleon dominates in the plateau region. We therefore use in all of our analysis $t_f - t_i \sim 1$ fm.

New inversions are necessary every time a different choice of the projection matrix Γ^α is made. In this work, we consider choices, which are optimal for the form factors considered. Namely we use the spatial Γ's and consider the spatial component of the current i.e. we extract the form factors from
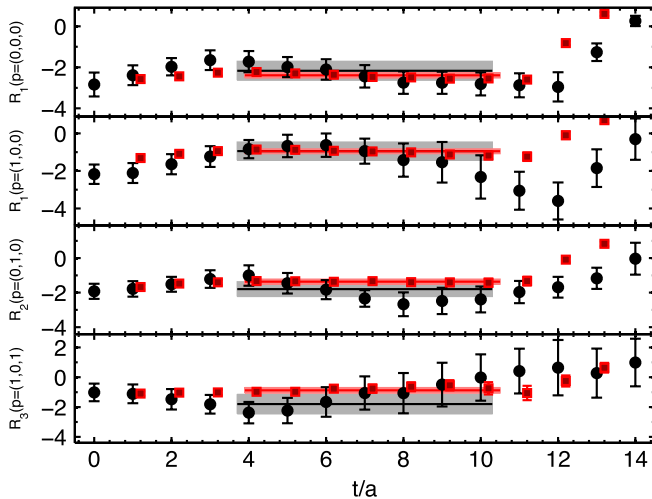

FIG. 2 (color online). The ratio of Eq. (12) for representative momentum combinations at $\beta = 3.9$ and different values of μ. The filled (black) circles show results with a sink-source separation $t_f/a = 14$ and the filled (red) squares for $t_f/a = 12$, shifted to the left by one time-slice.

$$\Pi^i(\Gamma^k, \vec{q}) = \frac{ic}{4m_N}\left[\frac{q_k q_i}{2m_N}G_p(Q^2) - (E + m_N)\delta_{i,k}G_A(Q^2)\right],$$

(14)

where $k = 1, 2, 3$, and $c = \sqrt{\frac{2m_N^2}{E(E+m_N)}}$.

B. Simulation details

The input parameters of the calculation, namely β, L/a and $a\mu$, are summarized in Table I. The lattice spacing a is taken from the nucleon mass as described in the next section. The pion mass values, spanning a mass range from 260 to 470 MeV, are taken from Ref. [29]. At $m_\pi \approx 300$ MeV and $\beta = 3.9$ we have simulations for lattices of spatial size $L = 2.1$ fm and $L = 2.8$ fm allowing to investigate finite size effects. Finite lattice spacing effects are studied using three sets of results at $\beta = 3.9$, $\beta = 4.05$ and $\beta = 4.2$ for the lowest and largest pion mass available in this work. These sets of gauge ensembles allow us to estimate all the systematic errors in order to produce reliable predictions for the nucleon axial form factors.

C. Determination of the lattice spacing

The nucleon mass has been computed on the same ensembles that are now used here for the computation of the nucleon axial form factors [13]. Therefore we can use the nucleon mass at the physical point to set the scale. We show in Fig. 3 results at three values of the lattice spacings corresponding to $\beta = 3.9$, $\beta = 4.05$ and $\beta = 4.2$. As can be seen, cutoff effects are negligible and we can therefore use continuum chiral perturbation theory to extrapolate to the physical point. For the observables discussed in this work the nucleon mass at the physical pion mass is the most appropriate quantity to set the scale. This also provides a cross-check for the determination of the lattice spacing by comparing with the value extracted from the pion decay constant. If lattice artifacts are under control then these two determinations should be consistent, under the assumption that quenching effects due to the absence of the strange quark from the sea are small for these quantities. In order to correct for volume effects we use chiral perturbation theory to take into account volume corrections coming from pions propagating around the lattice, following Ref. [30]. A similar analysis was carried out in Ref. [11] at $\beta = 3.9$ and $\beta = 4.05$ and we refer to this publication for further details. In addition, in this work we extend the analysis of Ref. [11] to include results at $\beta = 4.2$. In Table II we give the volume-corrected nucleon mass.

To chirally extrapolate we use the well-established $\mathcal{O}(p^3)$ result of heavy baryon chiral perturbation theory (HBχPT) given by

$$m_N = m_N^0 - 4c_1 m_\pi^2 - \frac{3g_A^2}{16\pi f_\pi^2}m_\pi^3.$$

(15)

TABLE I.   Input parameters ($\beta, L, a\mu$) of our lattice calculation and corresponding lattice spacing (a) and pion mass (m_π).

		$\beta = 3.9$, $a = 0.089(1)(5)$ fm, $r_0/a = 5.22(2)$			
$24^3 \times 48$, $L = 2.1$ fm	$a\mu$		0.0040	0.0064	0.0085	0.010
	Stat.		943	553	365	477
	m_π (GeV)		0.3032(16)	0.3770(9)	0.4319(12)	0.4675(12)
	$m_\pi L$		3.27	4.06	4.66	5.04
$32^3 \times 64$, $L = 2.8$ fm	$a\mu$	0.003	0.004			
	Stat.	667	351			
	m_π (GeV)	0.2600(9)	0.2978(6)			
	$m_\pi L$	3.74	4.28			

		$\beta = 4.05$, $a = 0.070(1)(4)$ fm, $r_0/a = 6.61(3)$		
$32^3 \times 64$, $L = 2.13$ fm	$a\mu$	0.0030	0.0060	0.0080
	Stat.	447	326	419
	m_π (GeV)	0.2925(18)	0.4035(18)	0.4653(15)
	$m_\pi L$	3.32	4.58	5.28

		$\beta = 4.2$, $a = 0.056(1)(4)$ fm $r_0/a = 8.31$	
$32^3 \times 64$, $L = 2.39$ fm	$a\mu$	0.0065
	Stat.	357
	m_π (GeV)	0.4698(18)
	$m_\pi L$	4.24
$48^3 \times 96$, $L = 2.39$ fm	$a\mu$	0.002
	Stat.	245
	m_π (GeV)	0.2622(11)
	$m_\pi L$	3.55

We perform a fit to the volume-corrected results at $\beta = 3.9$, $\beta = 4.05$ and $\beta = 4.2$ and extract $r_0 = 0.462(5)$ fm. Fitting instead to the $\beta = 3.9$ and $\beta = 4.05$ results we find $r_0 = 0.465(6)$ fm showing that indeed cutoff effects are small. To estimate the error due to the chiral extrapolation we use HBχPT to $\mathcal{O}(p^4)$, which leads to $r_0 = 0.489(11)$. We take the difference between the $\mathcal{O}(p^3)$ and $\mathcal{O}(p^4)$ mean values as an estimate of the uncertainty due to the chiral extrapolation. Fits to other higher order χPT
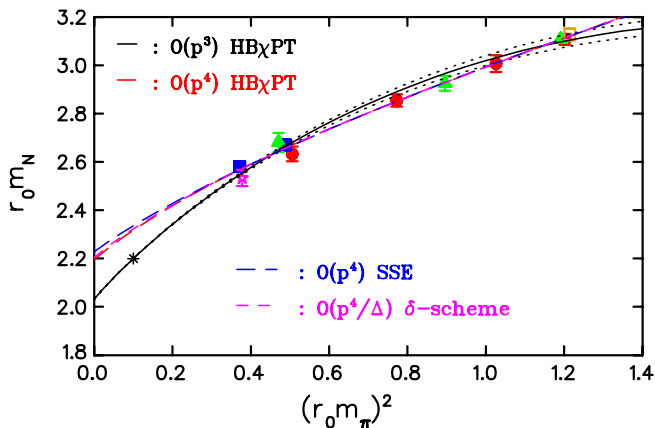

FIG. 3 (color online).   Nucleon mass in units of r_0 at three lattice spacings and spatial lattice size L such that $m_\pi L > 3.3$. The solid (black) and dashed (red) lines are fits to $\mathcal{O}(p^3)$ and $\mathcal{O}(p^4)$ HBχPT. The nucleon mass at the physical pion mass is shown with the asterisks. Results at $\beta = 3.9$ and $24^3 \times 48$ are shown with filled (red) circles, at $\beta = 3.9$ and $32^3 \times 64$ with the filled (blue) squares, at $\beta = 4.05$ and $32^3 \times 64$ with the filled (green) triangles, at $\beta = 4.2$ and $32^3 \times 64$ with the open (yellow) square and at $\beta = 4.2$ and $48^3 \times 96$ with the star (magenta).

TABLE II.   Results on the nucleon mass. The last column gives the values after a volume correction.

am_π	Lm_π	am_N	$am_N(L \to \infty)$
$\beta = 3.9$			
0.2100(5)	5.04	0.5973(43)	0.5952
0.1940(5)	4.66	0.5786(67)	0.5760
0.1684(2)	4.06	0.5514(49)	0.5468
0.1362(7)	3.27	0.5111(58)	0.5043
0.1338(2)	4.28	0.5126(46)	0.5115
0.1168(3)	3.74	0.4958(43)	0.4944
$\beta = 4.05$			
0.1651(5)	5.28	0.4714(31)	0.4702
0.1432(6)	4.58	0.4444(47)	0.4426
0.1038(6)	3.32	0.4091(60)	0.4056
$\beta = 4.2$			
0.1326(5)	4.24	0.380(3)	0.3763
0.0740(3)	3.55	0.306(4)	0.3049

formulas are also shown in Fig. 3. These are described in Ref. [13] and are consistent with $\mathcal{O}(p^4)$ HBχPT. Using $r_0 = 0.462(5)(27)$ fm and the computed r_0/a ratios we obtain

$$a_{\beta=3.9} = 0.089(1)(5) \text{ fm}, \qquad a_{\beta=4.05} = 0.070(1)(4) \text{ fm},$$

$$a_{\beta=4.2} = 0.056(2)(3) \text{ fm}.$$

These values are consistent with the lattice spacings determined from f_π and will be used for converting to physical units in what follows. We note that results on the nucleon mass using twisted mass fermions agree with those obtained using other lattice $\mathcal{O}(a^2)$ formulations for lattice spacings below 0.1 fm [11].

III. RESULTS

In the first subsection we discuss our results on the nucleon axial charge and in the second subsection we discuss the momentum dependence of the axial $G_A(Q^2)$ and the induced pseudoscalar $G_p(Q^2)$.

A. Axial charge

Our lattice results on the nucleon axial charge are shown in Fig. 4 and listed in Table III. In the same figure we also show results obtained using $N_F = 2 + 1$ domain wall fermions (DWF) by the RBC-UKQCD Collaborations [31] and using a mixed action with $2 + 1$ flavors of asqtad sea and domain wall valence fermions by LHPC [32]. The first observation is that results at our three different lattice spacings are compatible within error bars. The second observation is that results at two different volumes are also consistent. The third observation is that there is agreement among lattice results using different lattice actions even before taking the continuum and infinite volume limit.

1. Finite volume effects

In order to assess volume effects we plot in Fig. 5 results on g_A versus Lm_π. Besides TMF results we show the results obtained using $N_F = 2 + 1$ DWF [31] as well as within the mixed action approach [32]. As can be
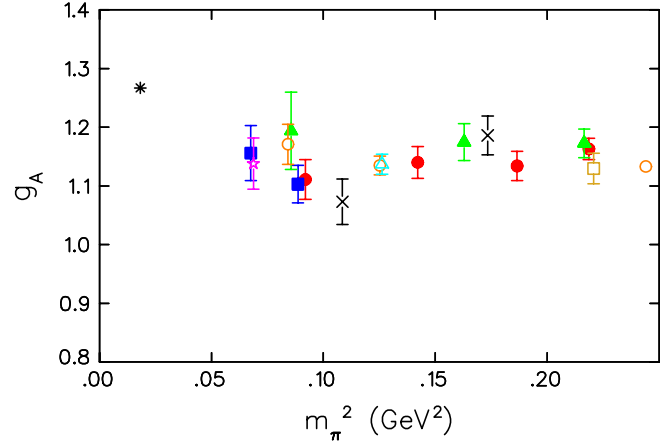

FIG. 4 (color online). The nucleon axial charge. Results using $N_F = 2$ twisted mass fermions are shown using the same notation as that of Fig. 3. Crosses show results obtained using $N_F = 2 + 1$ DWF, circles are results in a mixed action approach on a lattice of size $20^3 \times 64$ and the triangle on a lattice of size $28^3 \times 64$.

seen the results are consistent with a constant in the whole range of Lm_π spanned by our data. In particular we do not observe any decrease of g_A at values of Lm_π of about 3.3. Therefore, given that finite volume effects are negligible for the smallest value of $m_\pi L = 3.3$ as compared to the value we find at $m_\pi L = 4.3$, we conclude that for all of our data for which $m_\pi L > 3.3$ volume effects are small.

We can estimate the volume correction on g_A within heavy baryon chiral perturbation theory (HBχPT) in the so-called small scale expansion (SSE) [33], which includes explicitly the Δ degree of freedom. In this scheme one expands the results in powers of a small parameter ϵ, which denotes small pion four-momenta, the pion mass, baryon three-momenta and the nucleon-Δ mass splitting in the chiral limit. Writing

$$g_A(m_\pi, \infty) = g_A(m_\pi, L) - \Delta g_A(m_\pi, L) \qquad (16)$$

the dependence of g_A on the spatial length L of the lattice is given by [34]

$$
\begin{aligned}
\Delta g_A(m_\pi, L) = &-\frac{g_A^0 m_\pi^2}{4\pi^2 f_\pi^2} {\sum_{\vec{n}}}' \frac{K_1(L|\vec{n}|m_\pi)}{L|\vec{n}|m_\pi} + \frac{(g_A^0)^3 m_\pi^2}{6\pi^2 f_\pi^2} {\sum_{\vec{n}}}' \left[K_0(L|\vec{n}|m_\pi) - \frac{K_1(L|\vec{n}|m_\pi)}{L|\vec{n}|m_\pi} \right] \\
&+ \frac{c_A^2}{\pi^2 f_\pi^2} \left(\frac{25}{81} g_1 - g_A^0 \right) \int_0^\infty dy \, {\sum_{\vec{n}}}' \left[K_0(L|\vec{n}|f(m_\pi, y)) - \frac{L|\vec{n}|f(m_\pi, y)}{3} K_1(L|\vec{n}|f(m_\pi, y)) \right] \\
&+ \frac{8c_A^2 g_a^0}{27\pi^2 f_\pi^2} \int_0^\infty dy y {\sum_{\vec{n}}}' \frac{f(m_\pi, y)}{\Delta_0} \left[K_0(L|\vec{n}|f(m_\pi, y)) - \frac{K_1(L|\vec{n}|f(m_\pi, y))}{L|\vec{n}|f(m_\pi, y)} \right] \\
&+ -\frac{4c_A^2 g_A^0}{27\pi f_\pi^2} \frac{m_\pi^3}{\Delta_0} {\sum_{\vec{n}}}' \frac{1}{L|\vec{n}|m_\pi} e^{-L|\vec{n}|m_\pi} + \mathcal{O}(\epsilon^4)
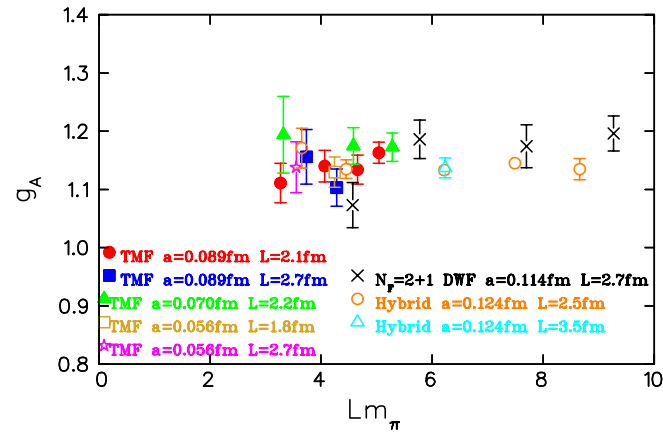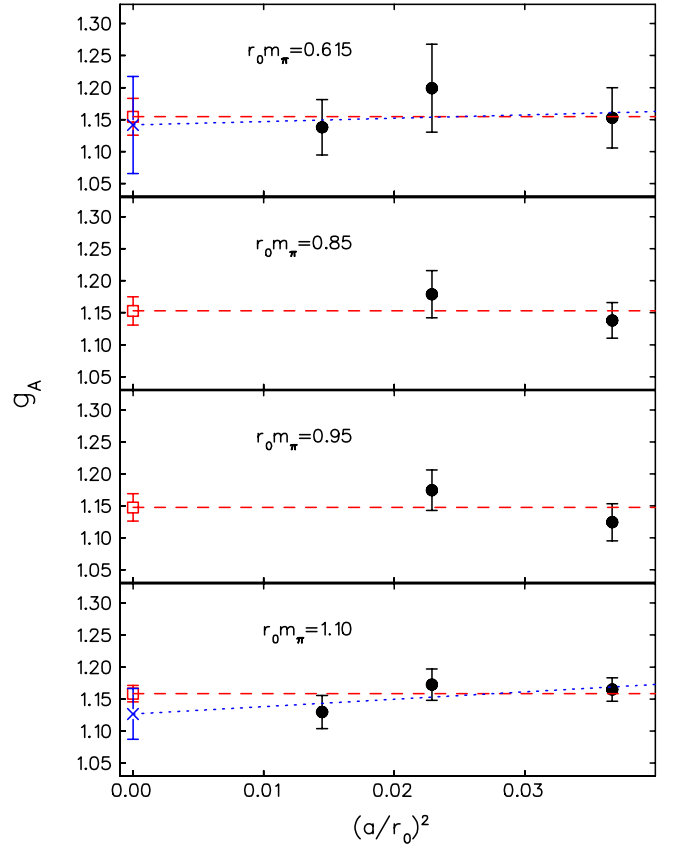\end{aligned}
\qquad (17)
$$

TABLE III. Results using $N_F = 2$ twisted mass fermions (TMF) on the axial nucleon charge. The last column gives the values after a volume correction.

m_π GeV	Lm_π	g_A	$g_A(L \to \infty)$
$\beta = 3.9$			
0.4675	5.04	1.163(18)	1.167
0.4319	4.66	1.134(25)	1.140
0.3770	4.06	1.140(27)	1.150
0.3032	3.27	1.111(34)	1.133
0.2978	4.28	1.103(32)	1.106
0.2600	3.74	1.156(47)	1.162
$\beta = 4.05$			
0.4653	5.28	1.173(24)	1.177
0.4035	4.58	1.175(31)	1.182
0.2925	3.32	1.194(66)	1.218
$\beta = 4.2$			
0.4698	4.24	1.130(26)	1.144
0.2622	3.55	1.138(43)	1.146

with $f(m_\pi, y) = \sqrt{m_\pi^2 + y^2 + 2y\Delta_0}$ and f_π the pion decay constant in the chiral limit which we approximate with its physical value i.e. we take $f_\pi = 0.092$ GeV. In the sum $\sum'_{\vec{n}}$ all vectors $\vec{n}$ are summed except $\vec{n} = \vec{0}$. In order to estimate the volume correction Δg_A we take the experimental value of the axial charge in the chiral limit i.e. $g_A^0 \sim g_A^{\text{exp}} = 1.267$ and the nucleon—Δ mass splitting in the chiral limit $\Delta_0 = 0.2711$ GeV. For the Δ axial coupling constant we use the SU(4) relation $g_1 = 9g_A^{\text{exp}}/5$ and for the nucleon to Δ axial coupling constants $c_A = 1.5$. The estimated volume-corrected g_A is given in Table III.

In order to assess cutoff effects we use the simulations at three lattice spacings at the smallest and largest pion mass used in this work. We take as the reference pion

FIG. 6 (color online). The nucleon axial charge as a function of the lattice spacing in units of r_0 at $r_0 m_\pi = 0.615$, $r_0 m_\pi = 0.85$, $r_0 m_\pi = 0.95$, $r_0 m_\pi = 1.10$, from top to bottom. We use $r_0 = 0.462(5)$ extracted from the nucleon mass. In the uppermost and lowermost graphs we show both the linear (dotted line) and constant fits (dashed line).

FIG. 5 (color online). The nucleon axial charge as a function of Lm_π. The notation is the same as that of Fig. 4.

mass the one computed on the finest lattice and interpolate results at the other two β-values to these two reference masses. In Fig. 6 we show the value of g_A at these reference pion masses computed in units of r_0. We perform a fit to these data using a linear form $g_A(a) = g_A(0) + c(a/r_0)^2$. The resulting fit is shown in Fig. 6. Setting $c = 0$ we obtained the constant line also shown in the figure. As can be seen, for both large and small pion masses the slope is consistent with zero yielding a value in the continuum limit in agreement with the constant fit. Therefore we conclude that finite a effects are negligible and for the intermediate pion masses we obtained the values in the continuum by fitting our data at $\beta = 3.9$ and $\beta = 4.05$ to a constant.

The g_A values found at six reference pion masses are given in Table IV. We display the continuum values obtained using a constant fit both when no volume corrections are included as well as when volume-corrected data are used. The volume-corrected data extrapolated to $a = 0$ are plotted in Fig. 7.

TABLE IV. In the second, third and fourth column we give the interpolated values of g_A at the value of $m_\pi r_0$ given in the first column. We used $r_0/a = 5.22(2)$, $6.61(3)$ and $8.31(5)$ for $\beta = 3.9$, 4.05 and 4.2, respectively. In the fifth column we give the value of g_A after extrapolating to $a = 0$ using a constant fit. In the parenthesis we give the corresponding values when using a linear fit. In the last column we give the continuum value of g_A for the volume-corrected data.

$r_0 m_\pi$	$g_A(\beta = 3.9)$	$g_A(\beta = 4.05)$	$g_A(\beta = 4.2)$	$g_A(a \to 0)$	$g_A(L \to \infty, a \to 0)$
1.1019	1.165(18)	1.173(25)	1.130(26)	1.159(13) [1.127(40)]	1.165(13) [1.144(40)]
1.0	1.132(25)	1.172(33)		1.147(20)	1.153(20)
0.95	1.125(29)	1.175(31)		1.148(21)	1.155(21)
0.85	1.138(28)	1.179(37)		1.153(22)	1.165(22)
0.686	1.110(39)	1.194(66)		1.127(34)	1.129(34)
0.615	1.153(47)	1.199(69)	1.138(43)	1.154(29) [1.142(76)]	1.165(29) [1.156(76)]

2. Chiral extrapolation

Our simulations cover a range of pion masses from about 470 MeV down to about 260 MeV. The pion mass dependence of the nucleon axial charge has been studied within HBχPT in the SSE formulation [35]. We use the one-loop result including explicitly the Δ degrees of freedom in order to extrapolate our lattice results to the physical point. We make a three parameter ansatz of the form

$$
g_A(m_\pi^2) = g_A^0 - \frac{(g_A^0)^3 m_\pi^2}{16\pi^2 f_\pi^2} + 4\Big\{ C_{\text{SSE}}(\lambda)
$$
$$
+ \frac{c_A^2}{4\pi^2 f_\pi^2}\Big[\frac{155}{972} g_1 - \frac{17}{36} g_A^0\Big] + \gamma \ln\frac{m_\pi}{\lambda}\Big\} m_\pi^2
$$
$$
+ \frac{4 c_A^2 g_A^0}{27\pi f_\pi^2 \Delta_0} m_\pi^2 + \frac{8}{27\pi^2 f_\pi^2} c_A^2 g_A^0 m_\pi^2 R(m_\pi)
$$
$$
+ \frac{c_A^2 \Delta_0^2}{81\pi^2 f_\pi^2}(25 g_1 - 57 g_A^0)
$$
$$
\times \Big\{\ln\frac{2\Delta_0}{m_\pi} - R(m_\pi)\Big\} + \mathcal{O}(\epsilon^4), \tag{18}
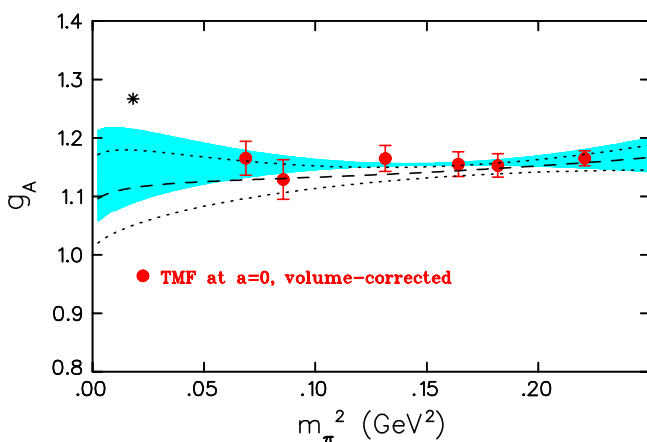$$

FIG. 7 (color online). The nucleon axial charge obtained by taking the continuum limit of the volume-corrected data. The shaded area shows the best fit to the data shown on the graph. The dashed line shows the best fit to the raw lattice data at the three values of β with the dotted lines being the associate error band.

with

$$
\gamma = \frac{1}{16\pi^2 f_\pi^2}\Big[\frac{50}{81} c_A^2 g_1 - \frac{1}{2} g_A^0 - \frac{2}{9} c_A^2 g_A^0 - (g_A^0)^3\Big]
$$
$$
= \sqrt{1 - \frac{m_\pi}{\Delta_0}}\Big[\frac{\Delta_0}{m_\pi} + \sqrt{\frac{\Delta_0^2}{m_\pi^2} - 1}\Big]. \tag{19}
$$

The three parameters to fit are g_A^0, the value of the axial charge at the chiral point, the Δ axial coupling constant g_1 and a counter-term $C_{\text{SSE}}(\lambda)$. We again take the nucleon to Δ axial coupling constant $c_A = 1.5$, the mass splitting between the Δ and the nucleon at the chiral limit, $\Delta_0 = 0.2711$ GeV and $\lambda = 1$ GeV. Fitting the volume-corrected continuum results we find $g_A = 1.12(8)$, $g_1 = 2.37(1.52)$ and $C_{\text{SSE}} = -1.01(2.01)$. The parameters g_1 and C_{SSE} are highly correlated explaining the resulting large error band. Fitting the lattice without any volume correction and without extrapolating to the continuum limit we obtained $g_A = 1.08(8)$, $g_1 = 2.02(1.21)$ and $C_{\text{SSE}} = -0.63(1.57)$ which are consistent with the continuum volume-corrected results. This shows that both cutoff and volume artifacts are small as compared to the uncertainty due to the chiral extrapolation.

B. Axial form factors

In this section we discuss the results obtained for the axial form factors $G_A(Q^2)$ and $G_p(Q^2)$.

To assess cutoff effects we compare in Fig. 8 results for $G_A(Q^2)$ and $G_P(Q^2)$ versus Q^2 for three different lattice spacings at a similar pion mass of about 470 MeV. As can be seen, results are consistent indicating that cutoff effects are negligible for these lattice spacings. We perform a dipole fit to $G_A(Q^2)$ using

$$
G_A(Q^2) = \frac{g_A}{(1 + Q^2/m_A^2)^2}, \tag{20}
$$

with a momentum upper range of $Q^2 \sim 1.5$ GeV^2. The axial mass m_A of the fits is larger than the experimental value $m_A^{\exp} = 1.1$ GeV extracted from the best dipole fit to the electroproduction data. This is evident from the smaller slope displayed by the lattice data both for twisted mass
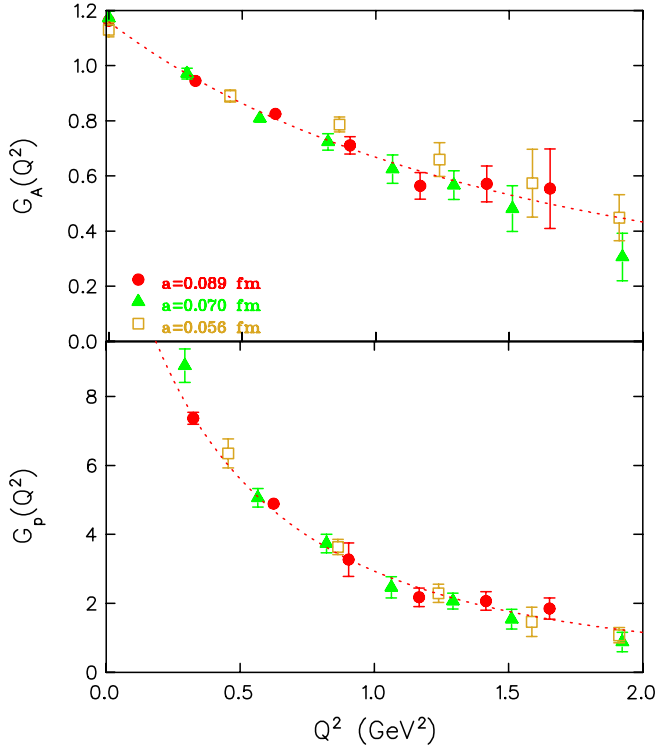
FIG. 8 (color online). The nucleon axial form factors $G_A(Q^2)$ and $G_p(Q^2)$ at $m_\pi \sim 470$ MeV at $\beta = 3.9$ (filled red circles), 4.05 (filled green triangles) and 4.2 (yellow squares) versus Q^2. The line is the result of a dipole fit (to the form given in Eq. (21)) $G_A(Q^2)$ ($G_p(Q^2)$) data on the coarse lattice.

fermions and domain wall fermions. Assuming the partially conserved axial current relation and pion-pole dominance we can relate the form factor $G_p(Q^2)$ to $G_A(Q^2)$:

$$G_p(Q^2) = G_A(Q^2)\frac{G_p(0)}{Q^2 + m_p^2}, \qquad (21)$$

where $G_p(0)$ and m_p are fit parameters.

The dependence of these form factors on the pion mass is seen in Fig. 9, where we plot both G_A and G_p computed at several values of the pion mass spanning a range from about 470 MeV to 300 MeV at $\beta = 3.9$. We show fits to the lattice data using a dipole form as given in Eq. (20) for $G_A(Q^2)$ and to the form given in Eq. (21) for $G_p(Q^2)$, which describe the Q^2 dependence of G_A and G_p rather well. Lattice results show a weaker Q^2 dependence as compared to experiment. Although the mass dependence is weak, the general trend of lattice results is to approach the experimental data as the pion mass is decreased. As already pointed out, the best dipole fit to the electroproduction data (solid line) yields an axial mass $m_A^{\text{exp}} = 1.1$ GeV [5], and it is shown by the solid line. The experimental line in the case of $G_p(Q^2)$ shown in Fig. 9 is obtained using Eq. (21) and taking m_p to be equal to the physical pion mass.
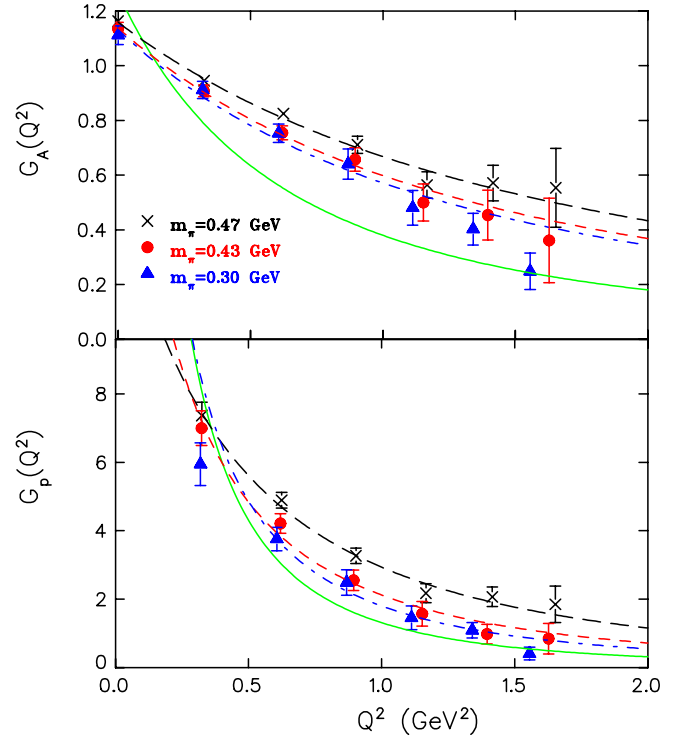
FIG. 9 (color online). The nucleon axial form factors $G_A(Q^2)$ and $G_p(Q^2)$ at $\beta = 3.9$ for $m_\pi = 468$ MeV (crosses), $m_\pi = 432$ MeV (filled red circles) and $m_\pi = 303$ MeV (filled blue triangles) versus Q^2. The dashed lines are the result of a dipole fit for $G_A(Q^2)$ and to the form given in Eq. (21) for $G_p(Q^2)$ on the coarse lattice. In the plot of $G_A(Q^2)$ the solid line is a dipole fit to the electroprodction data, where in the plot of $G_p(Q^2)$ the solid line is obtained from Eq. (21) by setting $m_p = 135 MeV$ and $G_p(0) = 4m_N^2$.

In Fig. 10 we check for finite volume effects by comparing results obtained at $\beta = 3.9$ on a lattice of spatial length $L = 2.8$ fm and $L = 2.1$ fm at $m_\pi \sim 300$ MeV. As can be seen volume effects are negligible for G_A. In the case of G_p we have a strong dependence on Q^2 as $Q^2 \rightarrow 0$ because of the pion-pole dependence expected for this form factor. Therefore the fits are strongly dependent on the available lowest Q^2 values. E.g. discarding the point at the lowest momentum yields the dotted lines which are steeper as compared to including it. Although there is an overall consistency between the two data sets at $\beta = 3.9$ deviations are seen in the fits when the same momentum range is used. The fit employing the whole range of data obtained on the smaller lattice, shown by the dashed red line, exhibits a weaker dependence as compared to the fit using the results on the larger lattice but discarding the point at the lowest momentum, shown by the dotted blue line. In Figs. 11 and 12 we compare our results with the results by LHPC which were obtained in a mixed action approach using DWF on staggered sea quarks [32] on a lattice with $L = 3.5$ fm. The results are in agreement in the case of
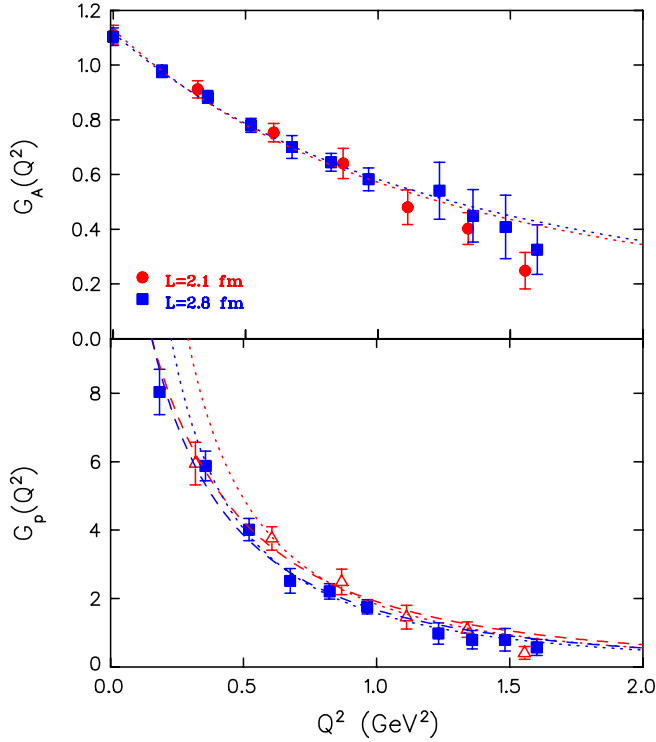
FIG. 10 (color online). The nucleon axial form factors G_A and G_p at $m_\pi \sim 300$ MeV for a lattice of size $24^3 \times 48$ (filled red circles) and $32^3 \times 64$ (filled blue squares). For $G_A(Q^2)$ (upper graph) the dotted lines are the best dipole fits to the lattice data. For $G_p(Q^2)$ (lower graph) the dotted lines are fits of lattice results to the form $\frac{CG_A(Q^2)}{(Q^2+m_p^2)}$ discarding the point at the lowest value of Q^2. The dashed lines are fits using all data points.
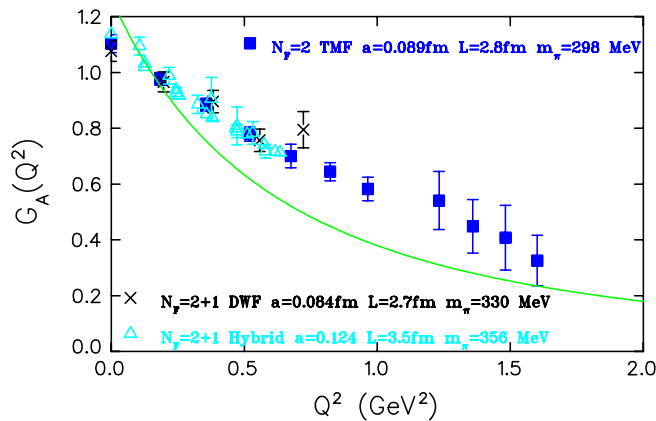

FIG. 11 (color online). Axial form factor $G_A(Q^2)$ as a function of Q^2. $N_F = 2$ TMF results at $m_\pi = 298$ MeV are shown with filled squares, $N_F = 2 + 1$ DWF with the crosses at $m_\pi = 330$ MeV and $N_F = 2 + 1$ using a mixed action of DWF and staggered sea quarks at $m_\pi = 356$ MeV with triangles. The solid line is the dipole parametrization of experimental data.
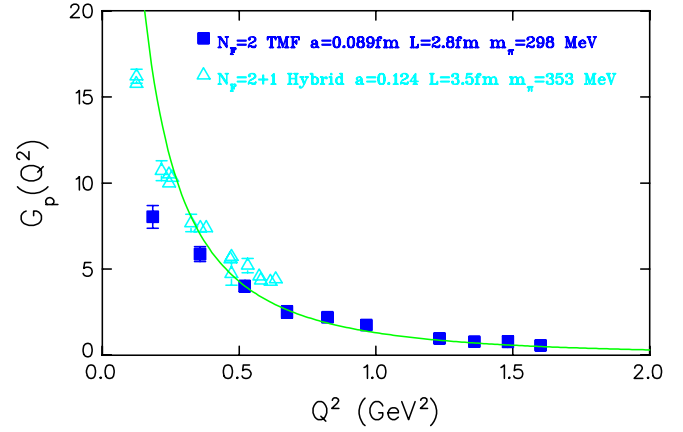

FIG. 12 (color online). Induced pseudoscalar form factor $G_p(Q^2)$ as a function of Q^2. $N_F = 2$ TMF results at $m_\pi = 298$ MeV are shown with filled squares and $N_F = 2 + 1$ using a mixed action of DWF and staggered sea quarks at $m_\pi = 356$ MeV are shown with triangles. The solid line is obtained using the parametrization of experimental electroproduction results for G_A and pion-pole dominance.

$G_A(Q^2)$, while in the case of $G_p(Q^2)$ there are larger discrepancies. Given the mass dependence of $G_p(Q^2)$ shown in Fig. 9 a difference in the pion mass of 50 MeV cannot fully account for this feature. Discrepancies of this kind may indicate that volume effects are not negligible on form factors such as $G_p(Q^2)$ which at low Q^2 are dominated by the pion-pole.

In the case of $G_p(Q^2)$ one can extract the fit parameters $G_p(0)$ and m_p by either fitting the G_p/G_A ratio or by using

TABLE V. Results on the axial nucleon charge and axial mass extracted by fitting $G_A(Q^2)$ to a dipole form. The two last column give the $G_p(0)$ and the mass m_p by fitting $G_p(Q^2)$ to the form given in Eq. (21).

$a\mu$	m_π (GeV)	g_A	m_A (GeV)	$G_p(0)$	m_p (GeV)
$\beta = 3.9$					
0.0100	0.4675	1.163(14)	1.776(48)	6.99(74)	0.738(77)
0.0085	0.4319	1.140(11)	1.634(32)	4.40(62)	0.458(106)
0.0064	0.3770	1.081(31)	2.021(17)	3.33(40)	0.254(113)
0.004	0.3032	1.135(34)	1.572(82)	4.30(76)	0.512(133)
0.004	0.2978	1.160(37)	1.513(70)	4.28(63)	0.459(119)
0.003	0.2600	1.166(28)	1.445(51)	2.80(25)	0.255(95)
$\beta = 4.05$					
0.008	0.4653	1.174(24)	1.696(24)	5.88(43)	0.595(53)
0.006	0.4035	1.174(32)	1.725(65)	4.90(84)	0.514(124)
0.003	0.2925	1.180(67)	1.392(44)	4.13(85)	0.458(153)
$\beta = 4.2$					
0.0065	0.4698	1.120(21)	2.030(93)	5.72(40)	0.599(60)
0.002	0.2622	1.158(22)	1.575(42)	3.56(18)	0.325(39)

C. ALEXANDROU *et al.*   PHYSICAL REVIEW D **83**, 045010 (2011)

the fitted values for $G_A(Q^2)$ and fitting to the form of Eq. (21). The values extracted by performing these fits are compatible within error bars. Our lattice data on $G_p(q^2)$ are flatter than pion-pole dominance predicts requiring a larger pole mass m_p than the pion mass measured on the lattice. In Table V we tabulate the resulting fitting parameters for all β and μ values. The parameters $G_p(0)$ and m_p have been extracted from fits to the form given in Eq. (21). The full set of our lattice results on $G_A(q^2)$ and $G_p(Q^2)$ is given in Tables VI, VII, and VIII of the Appendix.

IV. CONCLUSIONS

Using $N_F = 2$ twisted mass fermions we obtain accurate results on the axial $G_A(Q^2)$, and $G_p(Q^2)$ form factors as a function of Q^2 for pion masses in the range of about 260–470 MeV. The general feature of lattice data is a flatter dependence on Q^2 than experiment. This is a feature also seen in the electromagnetic nucleon form factors. Finite volume effects are found to be small on G_A. Our results are in agreement with recent results obtained using other lattice fermions such as dynamical $N_F = 2 + 1$ domain wall fermions. Having results at three lattice spacings enables us to take the continuum limit. We find that cutoff effects are small for the values of the lattice spacings used in this work. Performing a chiral extrapolation of our continuum results for the nucleon axial charge, we find at the physical point the value $g_A = 1.12(8)$. This is 1 standard deviation lower than the physical value. The large error associated with our determination of g_A is mostly due to the chiral extrapolation. Therefore it is crucial to perform an analysis with a pion mass closer to its physical value.

ACKNOWLEDGMENTS

We would like to thank all members of ETMC for a very constructive and enjoyable collaboration and for the many fruitful discussions that took place during the development of this work. Numerical calculations have used HPC resources from GENCI (IDRIS and CINES) Grant 2009-052271 and CC-IN$_2$P$_3$ as well as from the John von Neumann-Institute for Computing on the JUMP and Jugene systems at the research center in Jülich. We thank the staff members for their kind and sustained support. M. Papinutto acknowledges financial support by the Marie Curie European Reintegration Grant of the 7th European Community Framework Programme under Contract No. PERG05-GA-2009-249309. This work is supported in part by the DFG Sonderforschungsbereich/ Transregio SFB/TR9 and by funding received from the Cyprus Research Promotion Foundation under contracts EPYAN/0506/08, KY − Γ/0907/11/ and TECHNOLOGY/ ΘΕΠΙΣ/0308(BE)/17.

APPENDIX

TABLE VI. Results on the axial nucleon form factors at $\beta = 3.9$.

m_π (GeV) (no. confs)	$(aQ)^2$	G_A	G_p
$\beta = 3.9$, $24^3 \times 48$			
	0.0	1.163(18)	
	0.066	0.945(15)	7.368(390)
0.4675	0.126	0.825(19)	4.889(230)
(477)	0.182	0.711(31)	3.267(227)
	0.235(1)	0.564(48)	2.175(278)
	0.286(1)	0.571(65)	2.066(287)
	0.334(1)	0.554(14)	1.847(536)
	0.0	1.134(25)	
	0.065	0.908(22)	6.999(510)
0.4319	0.125	0.755(26)	4.211(287)
(365)	0.181(1)	0.657(43)	2.551(298)
	0.233(1)	0.499(68)	1.571(361)
	0.282(1)	0.454(91)	0.977(288)
	0.328(2)	0.361(154)	0.845(445)
	0.0	1.140(27)	
	0.065	0.931(24)	7.504(614)
0.3770	0.125	0.788(25)	4.145(325)
(553)	0.180(1)	0.737(74)	3.092(453)
	0.231(1)	0.648(211)	2.352(916)
	0.280(1)	0.631(202)	1.860(687)
	0.326(2)	0.329(292)	0.844(872)
	0.0	1.111(34)	
	0.064	0.911(31)	5.947(626)
0.3032	0.122	0.753(33)	3.757(341)
(943)	0.175(1)	0.640(55)	2.486(370)
	0.224(1)	0.480(63)	1.454(351)
	0.270(2)	0.402(58)	1.090(223)
	0.314(2)	0.248(67)	0.404(186)
$\beta = 3.9$,			**$32^3 \times 64$**
	0.00	1.103(32)	
	0.037	0.977(23)	8.040(660)
0.2978	0.072	0.884(23)	5.875(434)
(351)	0.105	0.779(25)	4.013(325)
	0.136	0.700(42)	2.518(361)
	0.166(1)	0.644(33)	2.208(222)
	0.195(1)	0.582(42)	1.758(208)
	0.249(1)	0.541(104)	0.977(314)
	0.274(2)	0.449(96)	0.792(271)
	0.299(2)	0.408(116)	0.791(330)
	0.323(2)	0.326(91)	0.569(238)

045010-10

TABLE VI. (*Continued*)

m_π (GeV) (no. confs)	$(aQ)^2$	G_A	G_p
	0.0	1.156(47)	
	0.037	0.967(31)	6.579(980)
0.2600	0.072	0.887(30)	5.441(488)
(667)	0.104	0.790(36)	3.976(462)
	0.135	0.628(46)	2.425(453)
	0.164(1)	0.589(39)	1.850(269)
	0.192(1)	0.507(42)	1.510(255)
	0.245(1)	0.403(60)	0.925(307)
	0.270(1)	0.335(62)	0.638(250)

TABLE VII. Results on the axial nucleon form factors at $\beta = 4.05$.

m_π (GeV) (no. confs)	$(aQ)^2$	G_A	G_p
$\beta = 4.05, 32^3 \times 64$			
	0.0	1.173(24)	
	0.037	0.971(19)	8.896(485)
0.4653	0.071	0.809(18)	5.063(269)
(419)	0.104	0.723(30)	3.735(269)
	0.134	0.625(51)	2.463(309)
	0.163	0.566(52)	2.064(229)
	0.191(1)	0.481(83)	1.540(289)
	0.243(1)	0.306(86)	0.879(283)
	0.268(1)	0.181(173)	0.310(319)
	0.0	1.175(31)	
	0.037	0.961(29)	8.213(645)
0.4032	0.071	0.842(32)	5.206(388)
(326)	0.103	0.792(56)	4.027(429)
	0.133	0.643(77)	2.224(415)
	0.161(1)	0.522(50)	1.499(215)
	0.188(1)	0.516(146)	1.563(485)
	0.238(1)	0.209(50)	0.584(188)
	0.262(1)	0.168(73)	0.420(204)
	0.0	1.194(66)	
	0.037	0.873(46)	7.165(1.089)
0.2925	0.070	0.735(47)	4.273(516)
(447)	0.101	0.557(73)	1.757(525)
	0.130(1)	0.540(110)	1.726(559)
	0.157(1)	0.509(194)	1.376(564)
	0.182(1)	0.383(103)	1.061(358)

TABLE VIII. Results on the axial nucleon form factors at $\beta = 4.2$.

m_π (GeV) (no. confs)	$(aQ)^2$	G_A	G_p
$\beta = 4.2, 32^3 \times 64$			
	0.0	1.130(26)	
	0.036	0.890(21)	6.348(422)
0.4698	0.069	0.786(270)	3.632(220)
(357)	0.099	0.659(61)	2.289(266)
	0.126	0.573(123)	1.462(422)
	0.152(1)	0.449(83)	1.073(221)
	0.177(1)	0.262(50)	0.535(114)
	0.222(1)	0.148(62)	0.225(123)
$\beta = 4.2, 48^3 \times 96$			
	0.0	1.138(43)	
	0.016	0.997(33)	11.392(882)
0.2622	0.032	0.856(23)	5.860(473)
(245)	0.046	0.759(28)	3.845(417)
	0.060	0.734(48)	3.212(358)
	0.072	0.634(30)	2.295(224)
	0.085	0.584(37)	1.604(188)
	0.108(1)	0.440(48)	1.260(217)
	0.119(1)	0.414(39)	0.946(151)
	0.129(1)	0.364(65)	0.604(181)
	0.139(1)	0.328(76)	0.452(201)

[1] L. A. Ahrens *et al.*, Phys. Lett. B **202**, 284 (1988).
[2] V. Bernard, N. Kaiser, and U. G. Meissner, Phys. Rev. Lett. **69**, 1877 (1992).
[3] S. Choi *et al.*, Phys. Rev. Lett. **71**, 3927 (1993).
[4] T. Gorringe and H. W. Fearing, Rev. Mod. Phys. **76**, 31 (2003).
[5] V. Bernard, L. Elouadrhiri, and U. G. Meissner, J. Phys. G **28**, R1 (2002).
[6] M. R. Schindler, T. Fuchs, J. Gegelia, and S. Scherer, Phys. Rev. C **75**, 025202 (2007).
[7] A. Shindler, Phys. Rep. **461**, 37 (2008); R. Frezzotti and G. C. Rossi, J. High Energy Phys. 08 (2004) 007.
[8] R. Frezzotti, P. A. Grassi, S. Sint, and P. Weisz (Alpha), J. High Energy Phys. 08 (2001) 058.
[9] P. Weisz, Nucl. Phys. **B212**, 1 (1983).
[10] C. Alexandrou, arXiv:0906.4137.
[11] C. Alexandrou *et al.* (ETM), Phys. Rev. D **80**, 114503 (2009).
[12] V. Drach *et al.*, Proc. Sci., LATTICE2008 (2008) 123.
[13] C. Alexandrou *et al.* (European Twisted Mass), Phys. Rev. D **78**, 014509 (2008).
[14] C. Alexandrou *et al.* (ETM Collaboration), Proc. Sci., LAT2007 (2007) 087 [arXiv:0710.1173].
[15] P. Dimopoulos, R. Frezzotti, C. Michael, G. C. Rossi and C. Urbach, Phys. Rev. D **81**, 034509 (2010).
[16] V. Drach *et al.*, Proc. Sci., Lattice 2010 (2010) 123.
[17] C. Alexandrou (ETM Collaboration), Proc. Sci., Lattice 2010 (2010) 001.
[18] C. Alexandrou *et al.*, Proc. Sci., LAT2009 (2009) 145 [arXiv:0910.3309].
[19] C. Alexandrou *et al.*, Proc. Sci., LAT2008 (2008) 145 [arXiv:hep-lat/9211042].
[20] P. Dimopoulos, R. Frezzotti, G. Herdoiza, C. Urbach, and U. Wenger (ETM Collaboration), Proc. Sci., LAT2007 (2007) [arXiv:0710.2498].
[21] M. Constantinou *et al.*, J. High Energy Phys. 08 (2010) 068.
[22] C. Alexandrou, M. Constantinou, T. Korzec, H. Panagopoulos, and F. Stylianou, Phys. Rev. D **83**, 014503 (2011).
[23] M. Constantinou, H. Panagopoulos, and F. Stylianou, Proc. Sci., LAT2009 (2009) 205 [arXiv:1001.1498].
[24] M. Gockeler *et al.*, Nucl. Phys. **B544**, 699 (1999).
[25] C. Alexandrou, M. Constantinou, T. Korzec, H. Panagopoulos, and F. Stylianou, Proc. Sci., LAT2010 (2010) 224 [arXiv:1012.2981].
[26] C. Alexandrou *et al.* (ETM Collaboration), Proc. Sci., LAT2009 (2009) 136.
[27] C. Alexandrou, S. Gusken, F. Jegerlehner, K. Schilling, and R. Sommer, Nucl. Phys. **B414**, 815 (1994).
[28] S. Gusken, Nucl. Phys. B, Proc. Suppl. **17**, 361 (1990).
[29] C. Urbach, Proc. Sci., LAT2007 (2007) 022.
[30] A. Ali Khan *et al.* (QCDSF-UKQCD), Nucl. Phys. **B689**, 175 (2004).
[31] T. Yamazaki *et al.*, Phys. Rev. D **79**, 114505 (2009).
[32] J. D. Bratt *et al.* (LHPC), Phys. Rev. D **82**, 094502 (2010).
[33] T. R. Hemmert, B. R. Holstein, and J. Kambor, J. Phys. G **24**, 1831 (1998).
[34] A. A. Khan *et al.*, Phys. Rev. D **74**, 094508 (2006).
[35] T. R. Hemmert, M. Procura, and W. Weise, Phys. Rev. D **68**, 075009 (2003).